Biochimica et Biophysica Acta 1787 (2009) 947–954

Contents lists available at ScienceDirect

Biochimica et Biophysica Acta

journal homepage: www.elsevier.com/locate/bbabio

# Modulation of mitochondrial $K^+$ permeability and reactive oxygen species production by the p13 protein of human T-cell leukemia virus type 1

Micol Silic-Benussi [a,1], Enrica Cannizzaro [a,1], Andrea Venerando [b], Ilaria Cavallari [a], Valeria Petronilli [c], Nicoletta La Rocca [d], Oriano Marin [e], Luigi Chieco-Bianchi [a], Fabio Di Lisa [c], Donna M. D'Agostino [a,f], Paolo Bernardi [c], Vincenzo Ciminale [a,f,*]

[a] Department of Oncology and Surgical Sciences, University of Padova, I-35128 Padova, Italy
[b] Venetian Institute of Molecular Medicine (VIMM), I-35129 Padova, Italy
[c] Consiglio Nazionale delle Ricerche Institute of Neuroscience at the Department of Biomedical Sciences, University of Padova, I-35121 Padova, Italy
[d] Department of Biology, University of Padova, I-35121 Padova, Italy
[e] Department of Biological Chemistry, University of Padova, I-35121 Padova, Italy
[f] Istituto Oncologico Veneto-IRRCS, I-35128 Padova, Italy

ARTICLE INFO

*Article history:*
Received 26 November 2008
Received in revised form 31 January 2009
Accepted 5 February 2009
Available online 11 February 2009

*Keywords:*
$K^+$ channel
Mitochondria
Permeability transition pore
Reactive oxygen species

ABSTRACT

Human T-cell leukemia virus type-1 (HTLV-1) expresses an 87-amino acid protein named p13 that is targeted to the inner mitochondrial membrane. Previous studies showed that a synthetic peptide spanning an alpha helical domain of p13 alters mitochondrial membrane permeability to cations, resulting in swelling. The present study examined the effects of full-length p13 on isolated, energized mitochondria. Results demonstrated that p13 triggers an inward $K^+$ current that leads to mitochondrial swelling and confers a crescent-like morphology distinct from that caused by opening of the permeability transition pore. p13 also induces depolarization, with a matching increase in respiratory chain activity, and augments production of reactive oxygen species (ROS). These effects require an intact alpha helical domain and strictly depend on the presence of $K^+$ in the assay medium. The effects of p13 on ROS are mimicked by the $K^+$ ionophore valinomycin, while the protonophore FCCP decreases ROS, indicating that depolarization induced by $K^+$ vs. $H^+$ currents has different effects on mitochondrial ROS production, possibly because of their opposite effects on matrix pH (alkalinization and acidification, respectively). The downstream consequences of p13-induced mitochondrial $K^+$ permeability are likely to have an important influence on the redox state and turnover of HTLV-1-infected cells.



## 1. Introduction

HTLV-1 is a complex retrovirus that infects an estimated 10–20 million people worldwide. HTLV-1 is the causative agent of an aggressive leukemia/lymphoma of mature $CD4^+$ T-cells termed adult T-cell leukemia/lymphoma (ATLL). ATLL arises in 1–5% of HTLV-1-infected subjects after a latency period of several decades and is refractory to current therapies. Despite intensive study, the molecular determinants of ATLL are incompletely understood (reviewed in ref. [1]).

Studies of the viral factors governing HTLV-1 replication and pathogenesis have been focused primarily on the transcriptional activator Tax, which plays a critical role in cell immortalization through its ability to deregulate the expression of a vast array of cellular genes and interfere with cell cycle checkpoints (reviewed in ref. [2]). Indeed, expression of Tax in mouse thymocytes is sufficient for induction of T-cell leukemia/lymphoma [3]. However, the contrast between the powerful oncogenic properties of Tax and the low prevalence and long latency of ATLL in HTLV-1-infected individuals suggests the existence of mechanisms that limit the transforming/pathogenic potential of the virus and favor life-long asymptomatic persistence in the host.

Recent studies indicate that the viral accessory proteins p12, p21, p30, HBZ and p13 also contribute to HTLV-1 replication and pathogenesis (reviewed in ref. [4]). The present study is focused on p13, an 87-amino acid accessory protein that is targeted to the inner membrane of mitochondria (reviewed in ref. [5]). In the context of cells, p13 induces mitochondrial fragmentation [6], slows down proliferation [7,8], promotes apoptosis triggered by ceramide and FasL [7,8], and interferes with tumor growth in experimental models [8]. Although competent for replication in tissue culture, a p13-knockout virus is incapable of establishing a persistent infection in a rabbit experimental model [9]. Biophysical and biochemical analyses

* Corresponding author. Dipartimento di Scienze Oncologiche e Chirurgiche, Università di Padova, via Gattamelata 64, I-35128 Padova, Italy. Tel.: +39 049 821 5885; fax: +39 049 807 2854.
*E-mail address:* v.ciminale@unipd.it (V. Ciminale).
[1] These authors contributed equally to the work.

0005-2728/$ – see front matter © 2009 Elsevier B.V. All rights reserved.
doi:10.1016/j.bbabio.2009.02.001

of a synthetic peptide spanning residues 9–41 ($p13^{9-41}$) indicated that this region folds into an amphipathic α-helix upon exposure to membrane-mimetic solutions and changes mitochondrial membrane permeability to $K^+$ [10]. The present study was aimed at further understanding the mechanism of p13 function through analyses of the effects of full-length synthetic p13 on energized mitochondria.

## 2. Materials and methods

### 2.1. Peptide synthesis

Full-length wild-type p13 (87-*mer*) and p13-AL, which contains alanines in the place of 4 arginines in the mitochondrial targeting signal/amphipathic alpha helical domain [10], were synthesized by a solid phase method on a polyethylene glycol polyacrylamide (PEGA) resin functionalized with the acid labile linker 4-hydroxymethylphenoxyacetic acid (Novabiochem), using an Applied Biosystems Model 433 automated peptide synthesizer. The fluoren-9-ylmethoxycarbonyl (Fmoc) strategy [11] was used throughout the peptide chain assembly, with 2-(1H-benzotriazol-1-yl)-1,1,3,3-tetramethyluronium hexafluorophosphate (HBTU) and 1-hydroxybenzotriazole (HOBt) or 2-(1*H*-7-azabenzotriazol-1-yl)-1,1,3,3-tetramethyl uronium hexafluorophosphate methanaminium (HATU) employed as coupling reagents. The side-chain protecting groups were as follows: *tert*-butyl for Ser, Thr, Tyr, Asp and Glu; *tert*-butyloxycarbonyl for Trp; trityl for His, Cys, Asn and Gln; 2,2,4,6,7-pentamethyldihydrobenzofuran-5-sulfonyl for Arg. Acetylation steps were carried out after every coupling involving hydrophobic residues. Peptide cleavage was performed by reacting the peptidyl-resins with 95% TFA/ethanedithiol for 3 h. Crude peptides were subsequently purified by two serial chromatographic steps on preparative C8 and C18 reverse phase HPLC columns. Molecular masses of the peptides were ascertained by mass spectroscopy with direct infusion on a Waters-Micromass ZMD-4000 Mass Spectrometer. The purity of the peptides was about 95% as evaluated by analytical reverse phase HPLC.

### 2.2. Assays on isolated mitochondria

Liver mitochondria isolated from albino Wistar rats weighing about 300 g were prepared by standard centrifugation techniques exactly as previously described [12]. Briefly, the liver was minced with scissors in isotonic sucrose buffer (250 mM sucrose, 10 mM Tris–HCL, 0.1 mM EGTA-Tris, pH 7.4), washed with sucrose buffer to eliminate residual blood, and then homogenized. The suspension was centrifuged at 600 ×*g* for 10 min to eliminate cells and large debris. The supernatant was collected and centrifuged at 7000 ×*g* for 10 min to pellet mitochondria, which were then resuspended in the same buffer and centrifuged again at 7000 ×*g* for 10 min. The resulting washed mitochondrial pellet was resuspended in a small volume of sucrose buffer and assayed for protein content using the Biuret protein determination assay.

To assess the uptake of p13 into mitochondria, the synthetic protein (100 nM final concentration) was added to a 1-mg aliquot of mitochondria previously diluted in 2 ml KCl buffer, and incubated at 37 °C for 5 min. Mitochondria were then pelleted by centrifugation at 7000 ×*g* for 10 min, washed with 2 ml KCl buffer, and centrifuged again. Resulting mitochondrial pellets were resuspended in sucrose-HEPES buffer [10] and incubated on ice for 2 min after addition of dimethyl sulfoxide (DMSO, 5%; serving as a control) or digitonin (0.05% or 0.5%, prepared in DMSO). The suspensions were then centrifuged at 17,500 ×*g* for 10 min and resulting supernatants and pellets were solubilized and analyzed by SDS-PAGE followed by electrotransfer to PVDF membrane (HyBond P, GE Healthcare). Sodium carbonate extraction assays were carried out as described previously [10]. For this treatment, washed pellets of mitochondria loaded with p13 were resuspended in 100 mM sodium carbonate, pH 11.5 and incubated for 30 min on ice. The sample was then adjusted to 1.6 M sucrose, overlaid with a step gradient of 1.25 M- and 250 mM sucrose, and centrifuged at 47,000 rpm for 2 h in an SW60.1 rotor (Beckman Instruments). The gradient fractions containing soluble proteins (i.e., the bottom 1.6 M sucrose layer) and membrane-inserted proteins (i.e., the 1.25 M sucrose layer plus 0.25–1.25 M sucrose interface) were precipitated using trichloroacetic acid and analyzed by SDS-PAGE followed by electrotransfer to HyBond P. Blots were probed with antibodies against p13 (rabbit anti-p13, raised against the synthetic protein), Porin (Calbiochem), and Hsp 60 (Santa Cruz) followed by horseradish peroxidase-conjugated secondary antibodies (Pierce) and developed with chemiluminescence detection reagents (Pierce Supersignal Pico). Chemiluminescent signals were detected by exposure to Hyperfilm (GE Healthcare) or with a BioRad ChemiDoc XRS imager.

Mitochondrial volume changes, membrane potential, ROS production, and the threshold for opening of the permeability transition pore (PTP) were measured in a PerkinElmer 650–40 spectrofluorimeter equipped with magnetic stirring and thermostatic control. Mitochondrial volume changes were measured in "swelling assays" as the change in 90° light scattering at 540 nm [13]. Membrane potential was assayed by measuring the change in fluorescence intensity of rhodamine 123 (Molecular Probes) added at a concentration of 300 nM [14]. The probe was excited at 503 nm, and emission was analyzed at 525 nm with the excitation and emission slits set at 2 and 5 nm, respectively. $O_2$ consumption was measured polarographically with a Clark oxygen electrode in a closed temperature-controlled 2-ml vessel equipped with magnetic stirring (Yellow Springs Instruments). These assays were performed at 25 °C in a 2-ml final volume containing 2 mg mitochondria (measured as total protein in the Biuret assay) and KCl buffer, pH 7.4 (125 mM KCl, 10 mM Tris-MOPS, pH 7.4, 1 mM Pi-Tris, 20 μM EGTA-Tris, 5 mM glutamic acid and 2.5 mM malic acid).

Production of ROS in mitochondria was measured using Amplex UltraRed (Molecular Probes), which reacts with $H_2O_2$ in a 1:1 stoichiometric ratio to produce the fluorescent product Resorufin. Mitochondria (2 mg) were resuspended in KCl buffer in the presence of 5 μM Amplex UltraRed reagent and 5 mg/ml horseradish peroxidase. The probe was excited at 563 nm and its emission was measured at 587 nm over a 5-min timeframe at 37 °C in the absence or presence of p13 and other treatments described in the text. The slopes (m) of the resulting traces were used to calculate changes in $H_2O_2$ production expressed as the ratio ($m_2/m_1$) where $m_2$ is the slope after the treatment and $m_1$ is the slope before the treatment.

The threshold for PTP opening was assessed by measuring the mitochondrial calcium retention capacity using the $Ca^{2+}$ indicator Calcium Green-5N (Molecular Probes) as described previously [15].

For electron microscopy isolated mitochondria were fixed overnight at 4 °C in 3% glutaraldehyde prepared in 0.1 M sodium cacodylate buffer (pH 6.9), post fixed for 2 h in 1% osmium tetroxide in the same buffer and then processed according to [16]. Ultrathin sections (80 nm) were cut with an ultramicrotome (Ultracut, Reichert-Jung, Wien, Austria), stained with lead citrate and observed with a transmission electron microscope (TEM 300, Hitachi) operating at 75 kV.

## 3. Results

### 3.1. p13 increases the permeability of mitochondria to $K^+$ and affects their ultrastructure

Fig. 1 shows the effects of full-length p13 on mitochondrial light scattering, a measure of mitochondrial shape and volume. Assays performed in isotonic KCl buffer (125 mM KCl) confirmed that p13 induced a dose-dependent change of mitochondrial light scattering, and comparison with the $p13^{9-41}$ peptide employed in previous studies indicates that full-length p13 was considerably more potent

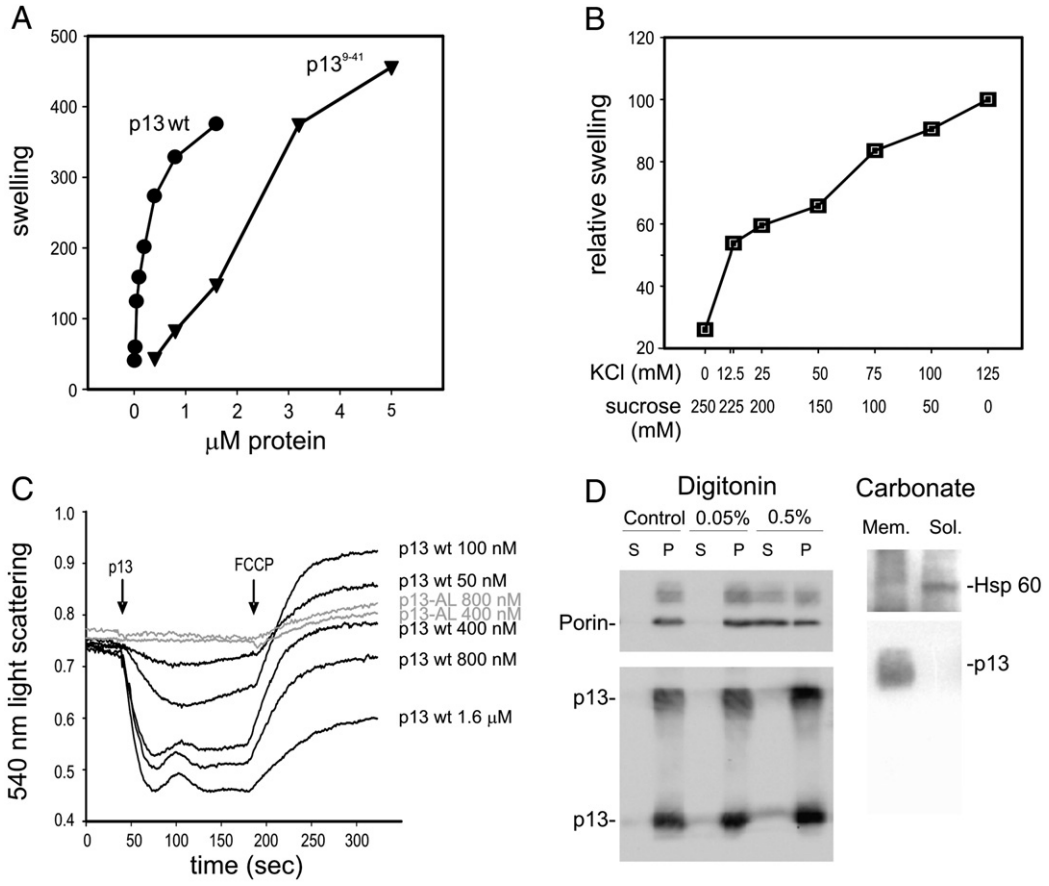


**Fig. 1.** Effects of p13 on $K^+$ permeability; submitochondrial targeting of p13. Rat liver mitochondria isolated as described in the text were placed in isotonic KCl buffer and treated with synthetic p13 protein. (A) Comparison of the light scattering change induced by full-length p13 (circles) and by a peptide spanning the alpha helical region of the protein [($p13^{9-41}$), triangles]. Values on the ordinate refer to the difference in light scattering at 540 nm measured after the addition of p13. Full-length p13 was tested at 12.5, 25, 50, 100, 200, 400, 800 and 1600 nM; $p13^{9-41}$ was tested at 400, 800, 1600, 3200 and 5000 nM. (B) Assays were carried out as described for panel A using 100 nM full-length p13 with the KCl and sucrose concentrations indicated on the abscissa. Values on the ordinate are scaled to a reference 100% light scattering change obtained in 125 mM KCl. (C) p13-induced changes of light scattering were reverted upon addition of 100 nM FCCP, which confirms their link to energy-dependent ion transport; in contrast, no effect on $K^+$ permeability was obtained with a p13 mutant carrying substitutions in the 4 critical arginine residues in the alpha helical domain of the protein (p13-AL). Results are representative of at least 3 experiments for each assay. Panel D shows results of digitonin and sodium carbonate extraction assays carried out to verify uptake of p13 into isolated mitochondria (see Materials and methods). Immunoblots were probed with antibodies against the indicated proteins and analyzed by chemiluminescent imaging (Digitonin panel) or exposure to autoradiographic film (Carbonate panel). As described in the Results, these assays indicated that p13 accumulated mainly in the inner mitochondrial membrane.

(Fig. 1A; see also ref. [10]). To test the dependence of the effects of p13 on the $K^+$ concentration, we carried out experiments in isotonic buffers containing increasing concentrations of $K^+$. Fig. 1B demonstrates that the effect induced by full-length p13 was strictly dependent on the KCl concentration.

Interestingly, the effects obtained with concentrations of p13 ranging from 50 nM to 400 nM were reversed after treatment with FCCP (Fig. 1C), a protonophore that collapses mitochondrial membrane potential ($\Delta\psi$). This finding is consistent with a $\Delta\psi$-dependent uptake of $K^+$ and indicates that the permeability increase induced by p13 is selective for $K^+$ vs. $H^+$ in this concentration range. In contrast, higher p13 concentrations (0.8 and 1.6 μM) resulted in only partial volume recovery after FCCP treatment (Fig. 1C), possibly reflecting a loss of selectivity which might have resulted in the transport of $Cl^-$ as well. Importantly, no light scattering changes were induced by the p13-AL mutant (Fig. 1C, grey traces), which carries substitutions of the 4 arginine residues in the alpha helical domain with alanine and leucine and is unable to induce mitochondrial morphological changes in cells [10].

To interpret the effects of p13 on mitochondrial parameters it was important to verify the uptake of synthetic p13 into isolated mitochondria, and the site of its accumulation, i.e., in the outer membrane, intermembrane space, matrix, or inner membrane, as documented previously for p13 expressed in transfected HeLa cells [10]. For this purpose, rat liver mitochondria were incubated with p13, washed, and then incubated with DMSO (5%, serving as a control) or digitonin (0.05% or 0.5%, prepared in DMSO). Resulting supernatants and pellets were analyzed by SDS-PAGE and immunoblotting to detect p13 and Porin, a marker for the outer mitochondrial membrane, which is expected to be solubilized by 0.5% digitonin. As shown Fig. 1D, a strong p13 signal (both monomer and multimer forms) was evident in the pellet fraction of mitochondria treated with DMSO or 0.05% digitonin. This observation verified that p13 was indeed taken up by isolated rat liver mitochondria in our in vitro assays. Treatment with 0.5% digitonin extracted a substantial portion of Porin; in contrast, p13 was detected almost exclusively in the pellet after this extraction. This result allowed us to exclude the outer membrane as the site of p13 accumulation.

To determine whether p13 taken up by mitochondria was membrane-inserted, which would indicate its accumulation in the inner membrane rather than the matrix or intermembrane space, we subjected p13-loaded mitochondria to sodium carbonate extraction [10]. Resulting fractions containing membrane-integrated proteins and soluble proteins were immunoblotted to detect p13 and Hsp 60 (a marker for a soluble mitochondrial protein). As shown in Fig. 1D, Hsp 60 was present mainly in the soluble fraction after carbonate

extraction, while p13 was detected in the membrane-associated fraction (as a multimer on this blot). Interpretation of these results together with those of the digitonin assay led us to conclude that p13 accumulated mainly in the inner mitochondrial membrane in our in vitro assays.

To gain insight into the basis for the light scattering changes induced by p13, we compared the ultrastructure of mitochondria subjected to treatment with p13 to that of mitochondria swollen through $Ca^{2+}$ mediated PTP opening. Results shown in Fig. 2 indicate that 100 nM p13 induced a shape change in mitochondria resulting in an electron-dense ring- or crescent-like morphology (Fig. 2C) that was clearly different from the large-amplitude swelling triggered by $Ca^{2+}$ (Fig. 2B), suggesting that the two processes leading to membrane permeabilization are distinct (see Discussion). Interestingly, in analogy with results observed in the light scattering assay (Fig. 1C), treatment with 100 nM p13 followed by FCCP resulted in a recovery of the original mitochondrial ultrastructure (Fig. 2D), suggesting that the basis for the shape changes was linked to energy-dependent $K^+$ transport. As shown in Fig. 2E, treatment with 800 nM p13, which triggered swelling that was only partially reversed by FCCP (see Fig. 1C), resulted in a substantial proportion of mitochondria that exhibited large-amplitude swelling similar to that observed using $Ca^{2+}$.

### 3.2. p13 influences mitochondrial membrane potential and electron transport chain (ETC) activity

If the process of $K^+$ influx induced by p13 is electrophoretic, it should cause inner membrane depolarization. This was tested using rhodamine 123, which is taken up by energized mitochondria in a potential-dependent manner [14]. Fig. 3A shows that p13 induced depolarization, with a marginal effect seen at low concentrations (50, 100 nM) and progressively more potent effects at higher concentrations (e.g. 1.6 μM) that nearly equaled the depolarization induced by FCCP. Interestingly, the p13-AL mutant had no effect on $\Delta\psi$ (Fig. 3A).

Electron transport through the ETC is coupled to proton extrusion. Therefore, membrane depolarization is predicted to stimulate electron transport and increase $O_2$ consumption. Closed-chamber polarographic measurements showed that p13 induced a dose-dependent increase in $O_2$ consumption when added up to a concentration of 400 nM (Fig. 3B). This effect leveled off at higher p13 concentrations, suggesting that other mitochondrial alterations might ensue, e.g. release of pyridine nucleotides or cytochrome *c*, which may result from swelling and outer membrane rupture [17]. This hypothesis is consistent with the reduced selectivity of the membrane permeability changes induced by p13 at high concentrations (see results in Fig. 1C). In analogy with its lack of permeabilizing activity in other assays, the p13-AL mutant did not affect $O_2$ consumption, nor did wild-type p13 when assayed in sucrose-based buffer lacking $K^+$, underscoring the strict $K^+$-selectivity of this effect.

We next tested whether increased proton extrusion resulting from the activation of the ETC might partially dampen p13′s effects on $\Delta\psi$ (Fig. 3C). To this end, we exposed mitochondria to rotenone, which blocks complex I of the ETC. As expected, rotenone induced partial depolarization. Pretreatment with p13 at 12.5 nM, i.e. a concentration unable to induce measurable depolarization *per se*, substantially increased rotenone-induced depolarization. This effect was more pronounced at 50 nM p13, which in the presence of rotenone induced

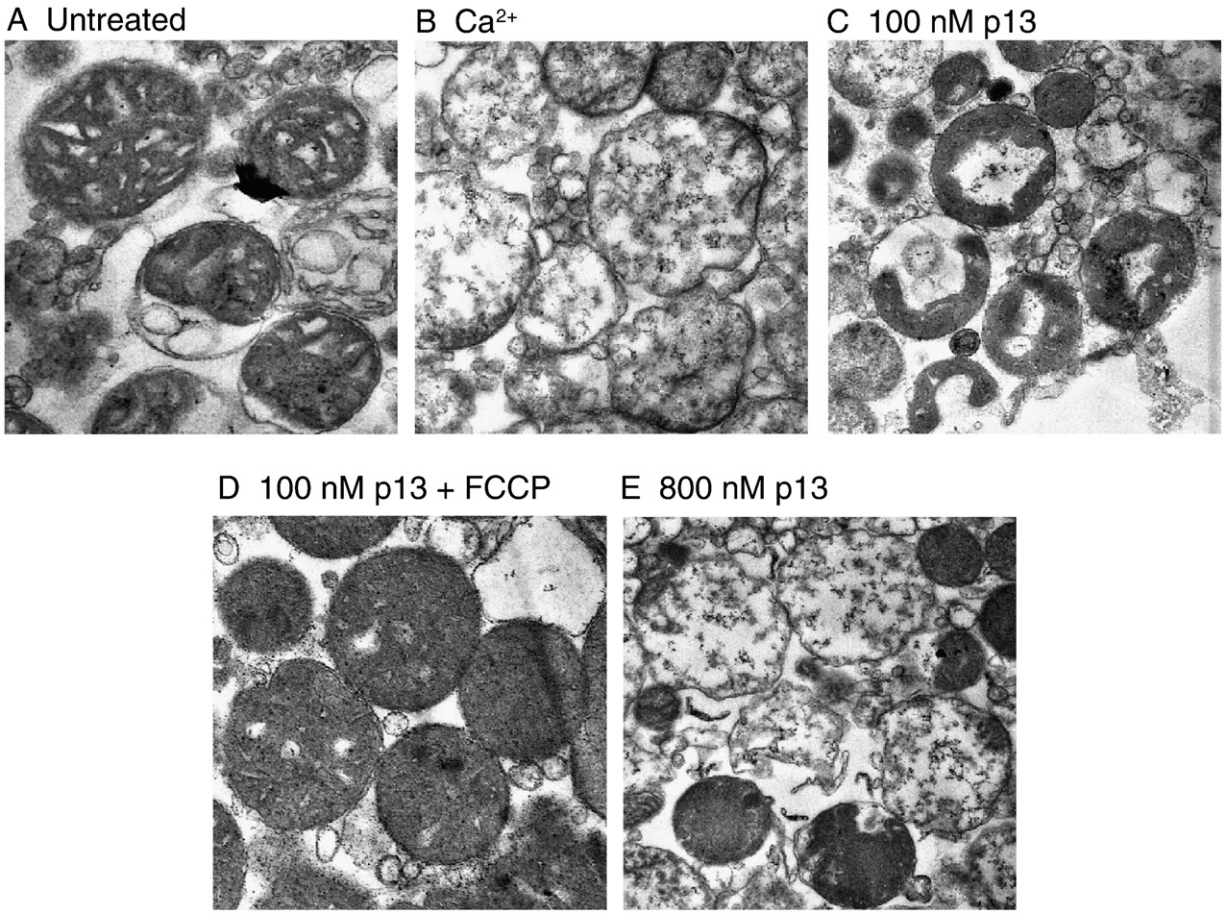


**Fig. 2.** Effects of p13 on mitochondrial ultrastructure. Results show the ring/crescent-like morphology of mitochondria treated with 100 nM p13 (C) in comparison to large amplitude swelling induced by $Ca^{2+}$ through PTP opening (B) or high doses of p13 (E). Effects of 100 nM p13 on ultrastructure were reverted by FCCP (D).

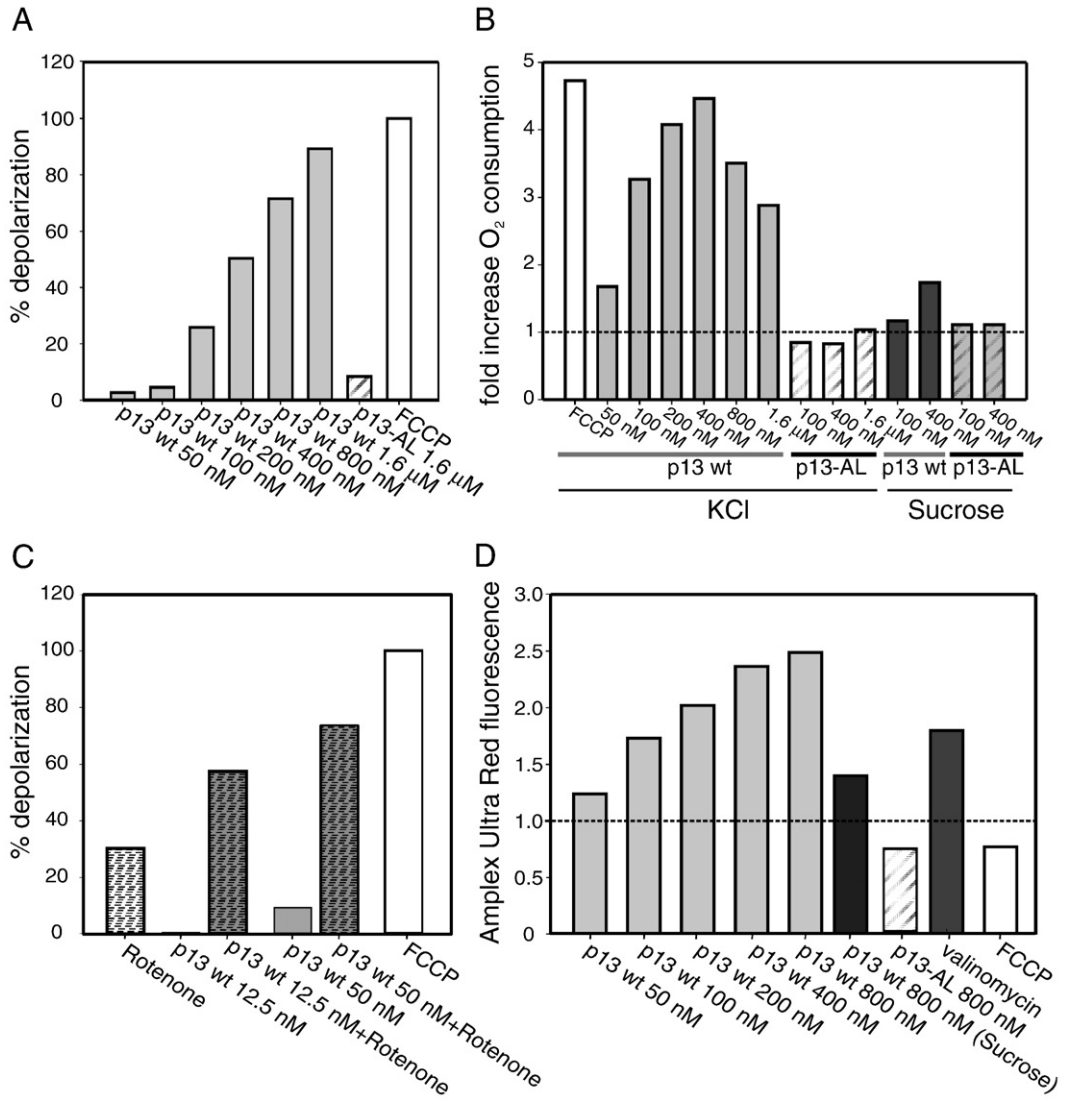


**Fig. 3.** Effects of p13 on mitochondrial membrane potential, respiration and ROS. (A) Effects of p13 on mitochondrial membrane potential. Depolarization is reported on the *y* axis as the change in rhodamine 123 fluorescence expressed as the percentage of the depolarization induced by 100 nM FCCP (set as 100%). (B) Effects of p13 on mitochondrial $O_2$ consumption. The *y* axis reports the fold change in the rate of $O_2$ consumption compared to the basal rate recorded in the absence of p13. (C) Inhibition of the ETC by rotenone enhances the depolarizing effects of p13. Depolarization is reported on the *y* axis as in panel A. The additive effect of the p13-induced depolarization and ETC inhibition by 2 μM rotenone is particularly evident at low concentrations of p13 that do not induce measurable depolarization *per se*. (D) Effects of p13 on mitochondrial $H_2O_2$, measured with the probe Amplex UltraRed. The *y* axis reports the ratio $m_2/m_1$, where $m_2$ and $m_1$ are the slopes of the traces after and before the indicated treatment, respectively. Results are representative of at least 3 experiments for each assay.

a depolarization that approached that obtained with FCCP. These data thus indicate that even low concentrations of p13 induce permeabilization to $K^+$ whose consequences on membrane potential and respiration fully emerge upon inhibition of the ETC.

### 3.3. Effects of p13 on ROS

As the ETC is a major source of ROS production in mitochondria, and since the amount of ROS produced depends on the rate of electron flux and the membrane potential, we reasoned that modulation of respiratory chain activity by p13 might be accompanied by a change in the levels of mitochondrial ROS. This possibility was tested using the $H_2O_2$ probe Amplex UltraRed. Fig. 3D reports the changes in probe fluorescence produced by different treatments, calculated as the ratio of the slopes after and before the treatment (see Materials and methods). Results showed that p13 induced a dose-dependent increase in ROS production (Fig. 3D). Interestingly, a similar effect was induced by the $K^+$ ionophore valinomycin. In contrast, treatment with FCCP reduced $H_2O_2$ production, suggesting that depolarization induced by $H^+$ vs. $K^+$ currents has opposite effects on ROS (see Discussion). Consistent with its dependence on $K^+$ transport, $H_2O_2$ production was not observed with the p13-AL mutant (Fig. 3D).

It is known that monoamine oxidases (MAO) associated with the outer mitochondrial membrane are also an important source of ROS in mitochondria [18]. To specifically measure $H_2O_2$ originating from the ETC we inhibited MAO activity using pargyline. Although this treatment did decrease the overall fluorescence intensity, p13 was still able to increase probe's fluorescence, indicating that its effects on ROS are independent of MAO activity (data not shown).

### 3.4. Effects of p13 on PTP gating

Both mitochondrial depolarization [19] and ROS [20] are known to affect the probability of opening of the PTP, a large conductance mitochondrial channel that triggers cell death through energy shortage and release of proapoptotic factors localized in the

intermembrane space [21,22]. To test whether p13 might affect PTP opening we employed the $Ca^{2+}$ retention capacity assay (see Materials and methods and ref [15]). This assay measures the sensitivity of the PTP to opening in response to $Ca^{2+}$, which is rapidly taken up by energized mitochondria. Uptake and release of $Ca^{2+}$ by mitochondria is measured using Calcium Green, a $Ca^{2+}$ probe that is excluded from mitochondria and therefore fluoresces when $Ca^{2+}$ is present outside mitochondria. Fig. 4A shows that addition of $Ca^{2+}$ resulted in its rapid uptake by mitochondria. The mitochondria were able to retain this dose of $Ca^{2+}$ until PTP opening was triggered by depolarization with FCCP (see trace in Fig. 4A) [23]. Remarkably, 400 nM p13 was also able to trigger PTP opening; in contrast, the p13-AL mutant had no effect. Further experiments carried out with serial additions of $Ca^{2+}$ allowed us to estimate the sensitivity of the PTP based on the concentration of $Ca^{2+}$ required to open it. Fig. 4B shows results of this analysis, expressed as the $Ca^{2+}$ retention capacity (CRC), which demonstrated that p13 reduced the CRC of mitochondria in a dose-dependent manner, indicating that the protein may indeed affect the threshold for PTP opening. Interestingly, treatment with the ROS scavenger mercaptopropionylglycine (MPG) partly inhibited the effect of p13, suggesting that the latter is, at least in part, ROS-dependent (Fig. 4C). Treatment of mitochondria with CsA resulted in an increase in CRC both in control and p13-treated mitochondria (Fig. 4C).

## 4. Discussion

The observations made in the present study support the working model of p13 function illustrated in Fig. 5. We have demonstrated that (i) p13 triggers an inward $K^+$ current into mitochondria (Fig. 1), ultrastructural changes (Fig. 2) and depolarization (Fig. 3A); (ii) depolarization induced by p13 enhances respiratory chain activity (Fig. 3B), which in turn partially dampens depolarization by increasing $H^+$ extrusion (Fig. 3C); (iii) these changes are accompanied by increased production of ROS (Fig. 3D) which, along with membrane depolarization, may (iv) be responsible for lowering the threshold of PTP opening (Fig. 4).

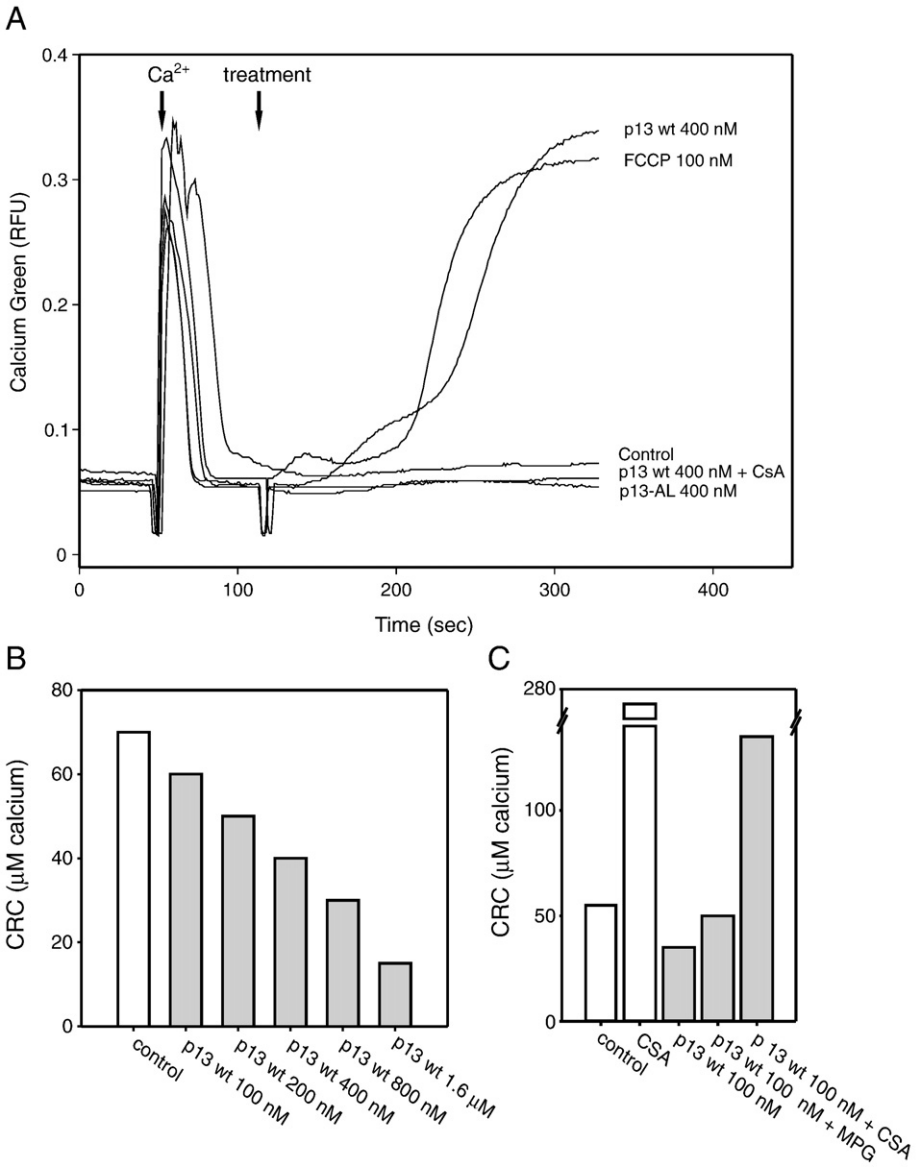


**Fig. 4.** Effects of p13 on the opening threshold of the PTP. Effects of p13 on PTP opening were assessed by measuring the $Ca^{2+}$ retention capacity (CRC) of isolated mitochondria (see text and ref. [15]). The same KCl isotonic incubation medium described for other in vitro assays was supplemented with 1 μM Calcium Green-5N. Panel A shows a time course experiment of $Ca^{2+}$ uptake and release following stimuli that trigger PTP opening. Panels B and C show the $Ca^{2+}$ concentration required to trigger PTP opening following treatment with increasing doses of p13 (B) and inhibition by CsA or ROS scavengers (C). RFU, relative fluorescence units. CRC, $Ca^{2+}$ retention capacity.

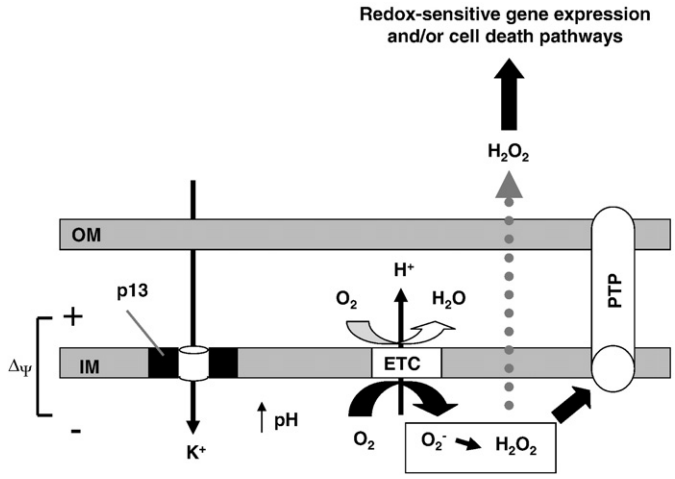


**Fig. 5.** Working model of p13 function. p13 forms or affects a $K^+$ channel in the inner mitochondrial membrane (IM) leading to $K^+$ influx in energized mitochondria. This induces depolarization that is partly compensated by activation of the respiratory chain and consequent increased extrusion of $H^+$. However, ETC activity also increases matrix pH and the chemical $H^+$ gradient, resulting in increased ROS production which, along with membrane depolarization, may lower the opening threshold of the PTP and trigger cell death. Increased $H_2O_2$ levels may also engage ROS-dependent "extramitochondrial" cell death pathways (e.g. ASK1/p38).

It remains to be determined whether p13 possesses intrinsic channel-forming activity or affects the activity of one of the described endogenous $K^+$ channels [24]. The first possibility is suggested by the previously documented ability of p13 to form multimeric structures in lipid-like environments [10], a property that has been described for channel-forming proteins termed viroporins that are coded by several other viruses [25].

A study by Hackenbrock [26] demonstrated a tight link between mitochondrial ultrastructure (and light scattering properties) and the oxidative phosphorylation/electron transport state as defined by Chance and Williams [27]. In contrast to large amplitude osmotic swelling which leads to outer membrane rupture, cristae unfolding, marked matrix expansion and loss of mitochondrial structure and function, the ultrastructural changes accompanying shifts in metabolic state are of smaller amplitude, and readily reversible. The most dramatic "state-coupled" change was observed in the state IV to state III transition in which ETC activity is dramatically boosted by addition of ADP in the presence of substrates. In this condition, Hackenbrock observed that the matrix condensed in a peripheral eccentric or ring-like structure surrounding an "internal compartment" apparently connected to the intermembrane space [26]. Interestingly, these ultrastructural changes and their reversibility closely match our observations made with low (e.g. 100 nM) concentrations of p13, suggesting that the ultrastructural changes induced by p13 are likely to result from a boost in ETC activity triggered by the inward $K^+$ current.

The finding that p13 triggers depolarization and increases ROS balance in isolated mitochondria may appear to be in contrast with previous studies suggesting that a decreased proton electrochemical gradient due to increased electron flux should be accompanied by reduced diversion of electrons from the ETC to oxygen, which should in turn result in decreased ROS production [28]. It is important to note that the data on which these conclusions are based were obtained either with the addition of protonophores or with activation of uncoupling proteins, i.e. under conditions where the depolarizing charge is carried by $H^+$, which will also cause matrix acidification and substrate depletion. In our studies the depolarizing current is carried by $K^+$, which causes a compensatory increase in $H^+$ pumping and will tend to increase matrix pH. Consistent with a key difference between depolarization by $H^+$ and $K^+$ currents, the effect of p13 on ROS production was mimicked by the $K^+$-selective ionophore valinomycin, while treatment with the protonophore FCCP resulted in the expected decrease in $H_2O_2$ production (Fig. 3D). Our findings are also consistent with recent data of Costa et al. showing that opening of the mitochondrial $K_{ATP}$ channel results in matrix alkalinization and increased $H_2O_2$ production [29].

Interestingly, mitochondrial generation of $H_2O_2$ was also demonstrated to occur during ceramide-induced apoptosis [30], a finding that suggests a link between the present work and previous results showing that expression of p13 in HeLa and Jurkat T cells was associated with an increased sensitivity to apoptosis induced by ceramide [7,8].

As shown in Fig. 4, p13 modulates the PTP and increases its sensitivity to opening. This effect can be traced to two synergistic mechanisms, i.e. (i) ROS-mediated shifting of the PTP voltage threshold [31], which is consistent with the recent demonstration that the pore plays a key role in the production of superoxide flashes *in situ* [32], and (ii) lowering of the membrane potential, which would draw the resting potential nearer to the opening threshold [33] (see [34] for a recent review on the relationship between mitochondrial $K^+$ channels and PTP regulation).

The ability of p13 to slow down cell growth [8] and sensitize cells to the apoptotic stimuli FasL and ceramide [7,8] suggests that this protein might limit the transforming potential of HTLV-1 in infected cells. This possibility is intriguing in light of the fact that Tax, the major HTLV-1-encoded oncoprotein, protects cells from apoptosis induced by mitochondria-mediated death stimuli [35,36]. Therefore Tax and p13 might exert opposite effects on cell turnover, on the one hand expanding the pool of infected cells and on the other hand limiting neoplastic transformation, thus favoring viral persistence and adaptation to the host. This hypothesis is consistent with the low frequency and long clinical latency of ATLL and with results of experiments carried out in a rabbit experimental model showing that p13 is required to establish a persistent infection in vivo [9]. Through its stimulation of ROS, p13 could also affect redox-sensitive gene expression, the consequences of which could either favor cell survival or promote cell death.

The accumulated data describing p13's biological properties reinforce the emerging concept that manipulation of mitochondrial function is a key point of convergence in tumor virus replication strategies. Indeed, recent studies have revealed that many viruses, including all of the human tumor viruses, express mitochondrial proteins [37,38]. Further investigations of p13 and its interactions with mitochondria may thus provide important insights into the mechanisms of HTLV-1 replication and pathogenesis and could aid in the discovery of new targets for anti-tumor therapy.

## Acknowledgments

We thank Prof. Antonio Toninello and Mario Mancon for supplying mitochondrial preparations for uptake assays. This work was supported by grants from the European Union ('The role of chronic infections in the development of cancer'; contract no. 2005-018704), Istituto Superiore di Sanità AIDS research program, the Associazione Italiana per la Ricerca sul Cancro (AIRC, grants to V.C. and P.B.), the Ministero per l'Università e la Ricerca Scientifica, e Tecnologica Progetti di Ricerca di Interesse Nazionale, by European Commission PRO-KINASERESEARCH 503467 and the University of Padova (grant to D.M.D.). E.C. was supported by a fellowship from AIRC.

## References

[1] K. Verdonck, E. Gonzalez, S. Van Dooren, A.M. Vandamme, G. Vanham, E. Gotuzzo, Human T-lymphotropic virus 1: recent knowledge about an ancient infection, Lancet, Infect. Dis. 7 (2007) 266–281.
[2] M.D. Lairmore, G. Franchini, Human T-cell leukemia virus types 1 and 2, In: D.M.K. a.P.M. Howley (Ed.), Fields Virology, Fifth Edition, vol. 2, Lippincott Williams and Wilkins, Philadelphia, 2007, pp. 2071–2106.

[3] H. Hasegawa, H. Sawa, M.J. Lewis, Y. Orba, N. Sheehy, Y. Yamamoto, T. Ichinohe, Y. Tsunetsugu-Yokota, H. Katano, H. Takahashi, J. Matsuda, T. Sata, T. Kurata, K. Nagashima, W.W. Hall, Thymus-derived leukemia-lymphoma in mice transgenic for the Tax gene of human T-lymphotropic virus type I, Nat. Med. 12 (2006) 466–472.
[4] C. Nicot, R.L. Harrod, V. Ciminale, G. Franchini, Human T-cell leukemia/lymphoma virus type 1 nonstructural genes and their functions, Oncogene 24 (2005) 6026–6034.
[5] D.M. D'Agostino, M. Silic-Benussi, H. Hiraragi, M.D. Lairmore, V. Ciminale, The human T-cell leukemia virus type 1 p13II protein: effects on mitochondrial function and cell growth, Cell Death Differ. 12 (Suppl 1) (2005) 905–915.
[6] V. Ciminale, L. Zotti, D.M. D'Agostino, T. Ferro, L. Casareto, G. Franchini, P. Bernardi, L. Chieco-Bianchi, Mitochondrial targeting of the p13II protein coded by the x-II ORF of human T-cell leukemia/lymphotropic virus type I (HTLV-I), Oncogene 18 (1999) 4505–4514.
[7] H. Hiraragi, B. Michael, A. Nair, M. Silic-Benussi, V. Ciminale, M. Lairmore, Human T-lymphotropic virus type 1 mitochondrion-localizing protein p13II sensitizes Jurkat T cells to Ras-mediated apoptosis, J. Virol. 79 (2005) 9449–9457.
[8] M. Silic-Benussi, I. Cavallari, T. Zorzan, E. Rossi, H. Hiraragi, A. Rosato, K. Horie, D. Saggioro, M.D. Lairmore, L. Willems, L. Chieco-Bianchi, D.M. D'Agostino, V. Ciminale, Suppression of tumor growth and cell proliferation by p13II, a mitochondrial protein of human T cell leukemia virus type 1, Proc. Natl. Acad. Sci. U. S. A. 101 (2004) 6629–6634.
[9] H. Hiraragi, S.J. Kim, A.J. Phipps, M. Silic-Benussi, V. Ciminale, L. Ratner, P.L. Green, M.D. Lairmore, Human T-lymphotropic virus type 1 mitochondrion-localizing protein p13(II) is required for viral infectivity in vivo, J. Virol. 80 (2006) 3469–3476.
[10] D.M. D'Agostino, L. Ranzato, G. Arrigoni, I. Cavallari, F. Belleudi, M.R. Torrisi, M. Silic-Benussi, T. Ferro, V. Petronilli, O. Marin, L. Chieco-Bianchi, P. Bernardi, V. Ciminale, Mitochondrial alterations induced by the p13II protein of human T-cell leukemia virus type 1. Critical role of arginine residues, J. Biol. Chem. 277 (2002) 34424–34433.
[11] G.B. Fields, R.L. Noble, Solid phase peptide synthesis utilizing 9-fluorenylmethoxycarbonyl amino acids, Int. J. Pept. Protein Res. 35 (1990) 161–214.
[12] P. Costantini, V. Petronilli, R. Colonna, P. Bernardi, On the effects of paraquat on isolated mitochondria. Evidence that paraquat causes opening of the cyclosporin A-sensitive permeability transition pore synergistically with nitric oxide, Toxicology 99 (1995) 77–88.
[13] V. Petronilli, C. Cola, S. Massari, R. Colonna, P. Bernardi, Physiological effectors modify voltage sensing by the cyclosporin A-sensitive permeability transition pore of mitochondria, J. Biol. Chem. 268 (1993) 21939–21945.
[14] R.K. Emaus, R. Grunwald, J.J. Lemasters, Rhodamine 123 as a probe of transmembrane potential in isolated rat-liver mitochondria: spectral and metabolic properties, Biochim. Biophys. Acta 850 (1986) 436–448.
[15] E. Fontaine, O. Eriksson, F. Ichas, P. Bernardi, Regulation of the permeability transition pore in skeletal muscle mitochondria. Modulation by electron flow through the respiratory chain complex i, J. Biol. Chem. 273 (1998) 12662–12668.
[16] N. Rascio, P. Mariani, E. Tommasini, M. Bodner, W. Larcher, Photosynthetic strategies in leaves and stems of *Egeria densa*, Planta 185 (1991) 297–303.
[17] F. Di Lisa, R. Menabo, M. Canton, M. Barile, P. Bernardi, Opening of the mitochondrial permeability transition pore causes depletion of mitochondrial and cytosolic $NAD^+$ and is a causative event in the death of myocytes in postischemic reperfusion of the heart, J. Biol. Chem. 276 (2001) 2571–2575.
[18] F. Di Lisa, M. Canton, R. Menabo, N. Kaludercic, P. Bernardi, Mitochondria and cardioprotection, Heart Fail. Rev. 12 (2007) 249–260.
[19] P. Bernardi, Modulation of the mitochondrial cyclosporin A-sensitive permeability transition pore by the proton electrochemical gradient. Evidence that the pore can be opened by membrane depolarization, J. Biol. Chem. 267 (1992) 8834–8839.
[20] P. Costantini, B.V. Chernyak, V. Petronilli, P. Bernardi, Modulation of the mitochondrial permeability transition pore by pyridine nucleotides and dithiol oxidation at two separate sites, J. Biol. Chem. 271 (1996) 6746–6751.
[21] A. Rasola, P. Bernardi, The mitochondrial permeability transition pore and its involvement in cell death and in disease pathogenesis, Apoptosis 12 (2007) 815–833.
[22] A.W. Leung, A.P. Halestrap, Recent progress in elucidating the molecular mechanism of the mitochondrial permeability transition pore, Biochim. Biophys. Acta 1777 (2008) 946–952.
[23] V. Petronilli, C. Cola, P. Bernardi, Modulation of the mitochondrial cyclosporin A-sensitive permeability transition pore. II. The minimal requirements for pore induction underscore a key role for transmembrane electrical potential, matrix pH, and matrix Ca2+, J. Biol. Chem. 268 (1993) 1011–1016.
[24] A. Szewczyk, J. Skalska, M. Glab, B. Kulawiak, D. Malinska, I. Koszela-Piotrowska, W.S. Kunz, Mitochondrial potassium channels: from pharmacology to function, Biochim. Biophys. Acta 1757 (2006) 715–720.
[25] M.E. Gonzalez, L. Carrasco, Viroporins, FEBS Lett. 552 (2003) 28–34.
[26] C.R. Hackenbrock, Ultrastructural bases for metabolically linked mechanical activity in mitochondria. I. Reversible ultrastructural changes with change in metabolic steady state in isolated liver mitochondria, J. Cell Biol. 30 (1966) 269–297.
[27] B. Chance, G.R. Williams, Respiratory enzymes in oxidative phosphorylation. III. The steady state, J. Biol. Chem. 217 (1955) 409–427.
[28] M.D. Brand, T.C. Esteves, Physiological functions of the mitochondrial uncoupling proteins UCP2 and UCP3, Cell. Metab. 2 (2005) 85–93.
[29] A.D. Costa, K.D. Garlid, I.C. West, T.M. Lincoln, J.M. Downey, M.V. Cohen, S.D. Critz, Protein kinase G transmits the cardioprotective signal from cytosol to mitochondria, Circ. Res. 97 (2005) 329–336.
[30] A. Quillet-Mary, J.P. Jaffrezou, V. Mansat, C. Bordier, J. Naval, G. Laurent, Implication of mitochondrial hydrogen peroxide generation in ceramide-induced apoptosis, J. Biol. Chem. 272 (1997) 21388–21395.
[31] V. Petronilli, P. Costantini, L. Scorrano, R. Colonna, S. Passamonti, P. Bernardi, The voltage sensor of the mitochondrial permeability transition pore is tuned by the oxidation-reduction state of vicinal thiols. Increase of the gating potential by oxidants and its reversal by reducing agents, J. Biol. Chem. 269 (1994) 16638–16642.
[32] W. Wang, H. Fang, L. Groom, A. Cheng, W. Zhang, J. Liu, X. Wang, K. Li, P. Han, M. Zheng, J. Yin, W. Wang, M.P. Mattson, J.P. Kao, E.G. Lakatta, S.S. Sheu, K. Ouyang, J. Chen, R.T. Dirksen, H. Cheng, Superoxide flashes in single mitochondria, Cell 134 (2008) 279–290.
[33] L. Scorrano, V. Petronilli, P. Bernardi, On the voltage dependence of the mitochondrial permeability transition pore. A critical appraisal, J. Biol. Chem. 272 (1997) 12295–12299.
[34] K. Nowikovsky, R.J. Schweyen, P. Bernardi, Pathophysiology of mitochondrial volume homeostasis: potassium transport and permeability transition, Biochim. Biophys. Acta (in press).
[35] D. Saggioro, S. Barp, L. Chieco-Bianchi, Block of a mitochondrial-mediated apoptotic pathway in Tax-expressing murine fibroblasts, Exp. Cell Res. 269 (2001) 245–255.
[36] R. Trevisan, L. Daprai, L. Acquasaliente, V. Ciminale, L. Chieco-Bianchi, D. Saggioro, Relevance of CREB phosphorylation in the anti-apoptotic function of human T-lymphotropic virus type 1 tax protein in serum-deprived murine fibroblasts, Exp. Cell Res. 299 (2004) 57–67.
[37] P. Boya, A.L. Pauleau, D. Poncet, R.A. Gonzalez-Polo, N. Zamzami, G. Kroemer, Viral proteins targeting mitochondria: controlling cell death, Biochim. Biophys. Acta 1659 (2004) 178–189.
[38] D.M. D'Agostino, P. Bernardi, L. Chieco-Bianchi, V. Ciminale, Mitochondria as functional targets of proteins coded by human tumor viruses, Adv. Cancer Res. 94 (2005) 87–142.